Journal of Power Sources 226 (2013) 334–339

Contents lists available at SciVerse ScienceDirect

Journal of Power Sources

journal homepage: www.elsevier.com/locate/jpowsour

Short communication

Enhanced electrical conductivity of $La_2Mo_{1.4}W_{0.6}O_9$ ceramic prepared by laser rapid solidification method

Jumei Yu [a,b], Mingju Chao [a,*], Dechuan Li [a], Mingyu Li [a]

[a] Key Laboratory of Materials Physics of Ministry of Education, School of Physical Science and Engineering, Zhengzhou University, Zhengzhou 450052, China
[b] Information and Engineering University of People's Liberation Army, Zhengzhou 450001, China

HIGHLIGHTS

- $La_2Mo_{1.4}W_{0.6}O_9$ oxygen ion conductor was prepared via laser rapid solidification.
- The ceramic material mainly grew paralleling to the laser incident direction.
- The ceramic material is of high electrical conductivity.
- Correlation between microstructure and conductivity was studied from brick layer model.

ARTICLE INFO

Article history:
Received 4 September 2012
Received in revised form
8 November 2012
Accepted 9 November 2012
Available online 17 November 2012

Keywords:
Oxygen ion conductor
Laser rapid solidification
Electrical conductivity
Grain boundary

ABSTRACT

A new method, laser rapid solidification, has been employed to prepare a kind of oxygen ion conductor—$La_2Mo_{1.4}W_{0.6}O_9$ ceramic. XRD and TGA measurements demonstrate that this material is of β-$La_2Mo_2O_9$ structure from room temperature to 800 °C. Images from scanning electron microscopy reveal that the sample is composed of relatively oriented large blocks paralleling to the laser incident beam and its microstructure is totally different from those of conventionally sintered ceramic. Results of AC impedance spectroscopy indicate that the influence of grain boundaries is little in the crystal solidification direction and the samples exhibit high electrical conductivity. For example, the values are 2.2×10^{-3} S cm^{-1}, 0.017 S cm^{-1}, 0.058 S cm^{-1} and 0.09 S cm^{-1} in dry air at 500 °C, 600 °C, 700 °C and 800 °C, respectively, which are about three to five times as high as those of samples prepared by solid state reaction method. It is suggested from the brick layer model that the main reason for the increase is the less grain boundary effect associated with the special microstructure of the samples.

1. Introduction

Oxygen ion conducting ceramics have a wide variety of applications in high temperature ionic devices, such as solid oxide fuel cells (SOFC), oxygen transport membranes and sensors, etc. As for SOFC, they are used as electrolyte. Most attractive electrolyte materials of SOFC include Y_2O_3 or Sc_2O_3-stabilized ZrO_2 (YSZ, SSZ), gadolinium-doped CeO_2 (GDC), Strontium and magnesium-doped $LaGaO_3$ (LSGM) and $La_2Mo_2O_9$-based ceramics [1]. To solve problems at high temperature and reduce application cost, it is critical to improve oxygen ionic conductivity of electrolyte materials at lower temperature (current target in research ~ 500 °C).

It has been well established that the microstructure of ceramic is closely related to processing methods and has great influence on its properties, including the electrical conductivity. In general, oxygen ion conducting ceramics are synthesized and sintered via solid state reaction method [2–4]. The process is simple, but high temperature and long time are essential for reaction and sintering, and there are several drawbacks such as limited degree of homogeneity and rather low relative density, which reduce the electrical conductivity. Wet chemical routes, such as modified sol–gel methods [5–8], freezing drying method [9–11], co-precipitation method [12], can be used to produce nano-structured precursors, which are of good homogeneity and can be sintered to higher dense ceramics at lower temperature. Though these methods are different in preparing precursors, long time sintering process is also necessary to obtain dense ceramics for all of them. In the sintering process, pressed solid powders grow little by little at high temperature to form ceramics consisting of many grains and grain boundaries. Therefore, their ionic conductivities are determined by

* Corresponding author. Tel.: +86 37167767836; fax: +86 37167766629.
E-mail addresses: yjm526@163.com (J. Yu), chaomingju@zzu.edu.cn (M. Chao), lidechuan2002@163.com (D. Li), my040075@163.com (M. Li).

0378-7753/$ – see front matter © 2012 Elsevier B.V. All rights reserved.
http://dx.doi.org/10.1016/j.jpowsour.2012.11.021

both the grains and the grain boundaries. Guo et al. reviewed the electrical properties of the grain boundaries of acceptor-doped zirconia and ceria in detail and drew a conclusion that the grain boundaries presented a blocking effect to the ionic transport across them and played a crucial part in conductivity especially below 600 °C [13]. Recently, laser has been used as heat source to prepare several bulk ceramics, such as several negative thermal expansion materials [14], solid oxide fuel cell electrolyte LSGM [15] and dielectric material $BaTi_2O_5$ [16] and so on. Since samples can be synthesized and solidify within a few minutes in the process, this method is called laser rapid solidification (denoted as LRS) and holds prospect for more applications. Furthermore, it is interesting that LSGM obtained by LRS has much higher electrical conductivity than those synthesized by solid state reaction route with similar purity and density [15]. However, the correlation between the character and the special microstructure of LSR samples needs further study.

The family of $La_2Mo_2O_9$-based materials exhibiting conductivity about 6×10^{-2} S cm^{-1} at 800 °C was reported by the group of Lacorre in 2000 [17]. The un-doped $La_2Mo_2O_9$ compound undergoes a structure transition from a high temperature cubic phase (β-$La_2Mo_2O_9$) to a low temperature monoclinic phase (α-$La_2Mo_2O_9$) at approximately 580 °C, with decrease of two orders of magnitude in the ionic conductivity [18,19]. And it also suffers from degradation in highly reducing atmosphere [20–22]. The phase transition and the chemical instability limit its application. Reports suggest that the ratio in mole of substitution of Molybdenum (Mo) by tungsten (W) is up to 80%, and when it is higher than 25%, the cubic phase can be stabilized to room temperature and the stability in reducing conditions can be enhanced [2,4,20–25]. In most of studies, $La_2Mo_2O_9$-based compounds are synthesized via solid state reaction route which involves several longtime heating processes at different temperatures from 500 °C to the final sintering temperature with intermediate regrinds to control the stoichiometric proportions and obtain a pure single phase sample [2,4,17,21,22,24]. Different precursor synthesis and sintering methods have also been studied [7,11], and results show that preparation methods make little difference in the conductivity of grain interiors but make a great difference in the conductivity of grain boundaries.

In this paper, LRS method is successfully employed to prepare dense $La_2Mo_{1.4}W_{0.6}O_9$ ceramic (labeled as LMW0.6 in the below), and the thermal stability, microstructure and electrical conductivity of samples and their correlation related to this special fabrication procedure are studied.

2. Experimental details

2.1. Synthesis

La_2O_3 (≥99.5%), MoO_3 (≥99.5%) and WO_3 (≥99.5%) were used as starting materials. La_2O_3 was fired in air at 800 °C for 3 h to ensure that it was free from absorbed species like moisture and CO_2 before being weighed. The desired ratio in mole of La:Mo:W was 2:1.4:0.6. The mixture was ground for 6 h with a pestle in a mortar and uniaxially pressed into disks of about 13 mm in diameter and 4 mm in thickness with a steel mould at 20 MPa. Next, the disks were fired for 5 h at 590 °C to avoid the sublimation of MoO_3. Then a disk on a horizontal tabulate stainless steel test bed was exposed to a beam of continuous-wave CO_2 laser of 5 mm in diameter. Fig. 1 is the diagrammatic sketch of the apparatus and a sample to be processed. Different laser powers of 600 W, 700 W and 800 W were employed in experiments and it was optimally controlled to increase smoothly from zero to 700 W in 30 s and keep stable for 80 s and then drop smoothly to zero in 30 s. As the laser power increased, the materials began to melt and took chemical synthesis

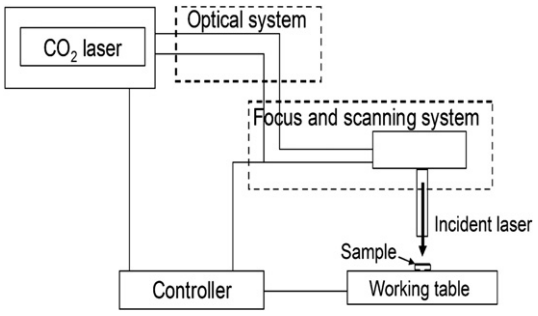

Fig. 1. Diagrammatic sketch of the apparatus and a sample to be processed by laser.

reaction. While the power was kept stable, the materials totally melted into a liquid drop and synthesis reaction continued. The horizontal position of the sample was shifted by a moving working table to have the materials irradiated uniformly in the process. As the laser was turned down and shut off, the materials rapidly solidified to a packed bulk roughly in the shape of a short cylinder. To ensure the thoroughness of the chemical synthesis reaction, the sample was cooled naturally in air to room temperature, then it was turned over and the same irradiating process was applied to the reversed face. After such a short time, a ceramic sample of about 8–10 mm in diameter and 3–3.5 mm in thickness could be obtained. For comparison, a series of LMW0.6 samples were prepared by conventional solid state reactions (denoted as SSR). Firstly, the ground powder was heated at 590 °C for 12 h and then was reground for 6–8 h. Secondly, it was heated at 800 °C for 12 h and was ground again. Then the powder was mixed with polyvinyl alcohol (PVA) and uni-axially pressed into disks with a steel mould at 80 MPa. Finally, the disks were kept respectively at 200 °C, 400 °C and 600 °C for 1 h to get rid of PVA and were sintered at 1050 °C for 12 h. The samples obtained were disks of about 12 mm in diameter and 1–2 mm in thickness.

2.2. Characterization methods

Both of the LRS and SSR samples were analyzed by XRD in the 2θ range of 15° ~75° at room temperature. The relative densities of the ceramic samples were measured via the Archimedes method. The thermal stability from room temperature to 800 °C was investigated in air at a heating rate of 10 °C/min with a thermogravimetric/differential thermal analyzer (TG/DTA). Microstructure

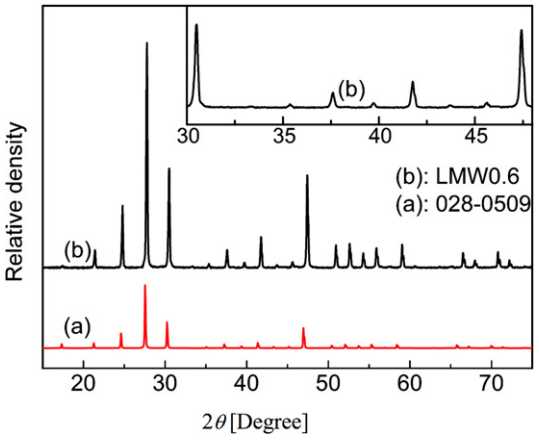

Fig. 2. XRD patterns of β-$La_2Mo_2O_9$ from JCPD 028-0509 (a) and LRS LMW0.6 (b). Inset shows details in the range of 30° ~48° of LRS LMW0.6.

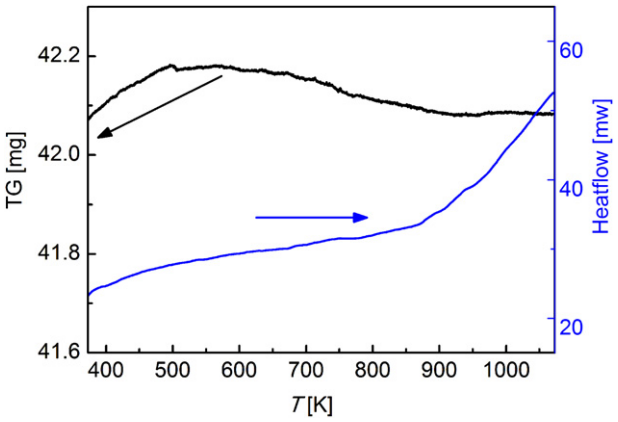

Fig. 3. TG-DTA curves of LRS LMW0.6.

observation and chemical analysis of the LRS samples were performed with JEOL JSM-6700F scanning electron microscope (SEM) equipped with Inca energy-dispersive spectrometer (EDS).

The electrical conductivity of samples was measured in dry air as a function of temperature (450–800 °C) by AC impedance spectrum with Pastat 2273 (Princeton Applied Research). The electrical conductivity of the LRS samples was investigated in two directions, parallel and perpendicular to the incident laser beam. Silver paste and silver nets were fired as electrodes. An LRS sample was sanded to a disk of 35.41 mm^2 in electrode's area and 3.22 mm in length for the measurement in the paralleling direction (denoted as $LRS_{\parallel}$), and another one for the perpendicular direction measurement (denoted as $LRS_{\perp}$) was sanded to a cuboid of 7.48 mm × 2.96 mm in electrode's area and 5.68 mm in length, and an SSR sample was sanded to a disk of 102.41 mm^2 in electrode's area and 1.28 mm in length. The range of AC frequency is 0.1 Hz–10^6 Hz. The data points of impedance were collected with an interval of 25 °C and the specimen was kept at a certain temperature for at least 15 min to equilibrate before measurement.

3. Results and discussion

3.1. XRD analysis and thermal analysis

The XRD powder patterns of the LRS ceramic and JCPD 028-0509 are shown in Fig. 2, which are in good agreement. The XRD patterns of α- and β-$La_2Mo_2O_9$ are quite similar and only the monoclinic α-phase exhibits some splitting diffraction peaks around $2\theta = 21.5°$, 27.9°, 30.6° and 47.6° [26]. From the enlarged peaks between 30°∼43° in the inset graph of Fig. 2, no splitting peaks can be observed. It reveals that LMW0.6 prepared by LRS method is of β-$La_2Mo_2O_9$ structure at room temperature. The phase of SSR samples is also confirmed to be β-$La_2Mo_2O_9$ structure. Fig. 3 shows the TG-DTA thermogram of the laser sintered LMW0.6. The mass is almost stable and no peak attributable to a phase transition is present, indicating that the phase transition has been completely suppressed. This fits the XRD results and published reports well [23,24].

Table 1
EDS results corresponding to the part shown in Fig. 4 (all results in atomic%).

Spectrum	Mo	La	W
Theoretical	10.77	15.38	4.62
1	10.44	15.18	4.55
2	10.71	15.31	4.61
3	10.82	15.51	4.69
4	10.51	15.04	4.42
Mean	10.62	15.26	4.57
Std. deviation	0.18	0.20	0.11

3.2. SEM and EDS analysis

As the power of laser beam increased during the irradiating process, materials under illumination formed a molten pool and took chemical reaction. And while the power reduced, the liquid product solidified rapidly. Since heat transfers mainly from the top surface to the bottom during the cooling process with strong temperature gradient, the crystal solidified parallel to the direction. Fig. 4 is the typical cross-section SEM image of the LMW0.6 sample prepared by LRS method. Here the cross-section is approximately perpendicular to the surface. It is clear that the crystal growth is relatively oriented along the direction from the bottom to the surface. The grains are over 100 μm long and densely packed without apparent pores. EDS results are shown in Table 1, which reveals the reaction is complete and uniform. In the conventional sintering process, pressed solid powders grow little by little at high temperature to form ceramics consisting of many grains and grain

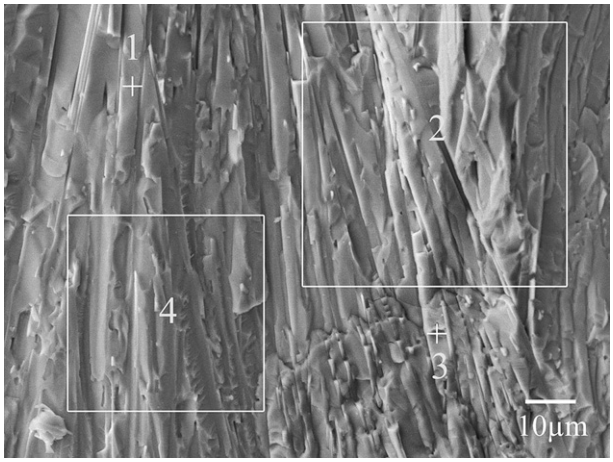

Fig. 4. Typical cross-section SEM image of LRS LMW0.6.

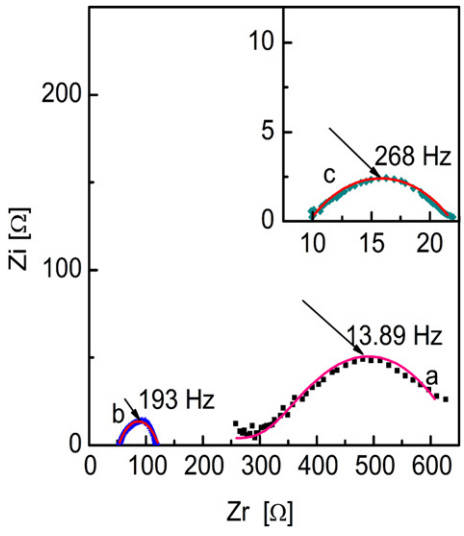

Fig. 5. Measured (scatter) and calculated (line) impedance spectra at 500 °C (a), 600 °C (b) and 800 °C (c) in dry air of $LRS_{\parallel}$ LMW0.6. Characteristic frequencies ω_0 are marked.

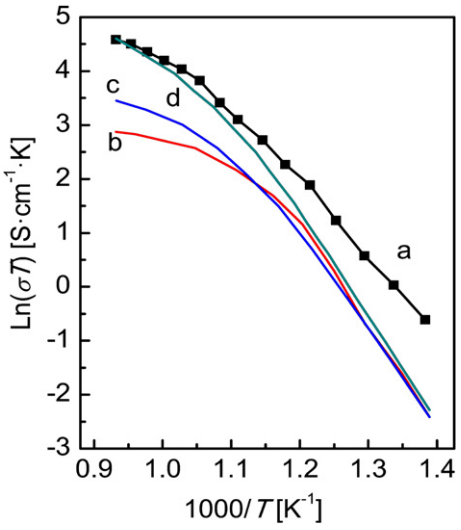

Fig. 6. Arrhenius plots in dry air of $LRS_{\|}$ LMW0.6 (a), $La_2Mo_{1.5}W_{0.5}O_9$ (b) and $La_2Mo_{1.25}W_{0.75}O_9$ (c) by Georges et al. [22], $La_2Mo_{1.5}W_{0.5}O_9$ (d) by Marrero-López et al. [23].

boundaries. Due to their different growth mechanisms, the microstructure of the laser sintered samples is totally different from those conventionally sintered ceramics. The measured relative densities of the SSR and LRS samples are around 96.2 and 98.6%, respectively.

3.3. Electrical conductivity

In general, an SOFC electrolyte obtained by conventional sintering method with porous silver paste electrodes is equivalent to a circuit of (*RQ*)(*RQ*)(*RQ*), three *RQ* elements in series corresponding to grain, grain boundary and material/electrode contribution. Here *RQ* elements consist of a resistance *R*, a capacitance *C*, and a CPE (constant phase element) in parallel. The corresponding impedance spectrum usually shows three arcs, in which the higher, medium and lower frequency arcs represent the grain interior impedance, the grain boundary impedance and the electrode polarization effect, respectively [9,11]. However, many factors can affect the shape of a spectrum. In fact, it is common that there are no arcs ascribed to the grain interior and the grain boundary responses owing to the fact that their characteristic frequencies are beyond the measurement range, especially at high temperature. In some cases, the medium frequency arc will not be present if the grain boundary resistance of the sample is little. Therefore, equivalent circuits *R*(*RQ*)(*RQ*), (*RQ*)(*RQ*) or *R*(*RQ*) will accordingly be chosen. In our experiment, impedance spectra were collected from 450 °C to 800 °C. The impedance spectra of the $LRS_{\|}$ sample collected at 500 °C, 600 °C and 800 °C are depicted in Fig. 5 as examples. There are two incomplete depressed arcs in the spectra measured below 500 °C, and they are fitted to *R*(*RQ*)(*RQ*) to obtain the resistance *R*, the pseudo-capacitance *Q*, (characterized by two parameters, *C* and *n*) by using ZSimpWin 3.0 software. To investigate the respective contribution of the grain interior, the grain boundary and the electrodes, capacitances are calculated from the relation $\omega_0 = (RQ)^{-1/n} = (RC)^{-1}$ [9]. Here ω_0 is the characteristic frequency, *C* is the true capacitance. Below 500 °C, the values of the capacitance associated with the high frequency arcs are among 1.48–8.92 × 10^{-11} F, indicating bulk response. Associated with the low frequency arcs, the values are among 16–335 μF, corresponding to electrode effect. As the temperature grows above 500 °C, only one arc in low frequency is visible in each of the spectra. Fitting them to the equivalent circuit *R*(*RQ*) and calculating as above, we get the results that the corresponding capacitances are among 9.4–46.8 μF, also with the order of magnitude due to electrode effect. That means the grain boundary effect is too little to be shown in AC impedance spectra in the whole measurement temperature range.

Therefore, the total resistance *R* of the $LRS_{\|}$ sample is determined according to the fitting value of the high frequency intercept of the impedance spectra with the real axes [9,15] and the conductivity value is calculated from $\sigma = L/RA$, where *L* is the thickness and *A* is the surface area of an electrolyte that is equal to the electrode area in our experiment. Arrhenius plot of the sample is given in Fig. 6. Consistent with the stabilization of the cubic symmetry at room temperature, the jump in conductivity at the α/β phase transition in $La_2Mo_2O_9$ is suppressed. The electrical conductivity studies by Georges et al. about $La_2Mo_{1.5}W_{0.5}O_9$ and $La_2Mo_{1.25}W_{0.75}O_9$ [22] and that by Marrero-López et al. on $La_2Mo_{1.5}W_{0.5}O_9$ [23] are chosen to be compared. Georges prepared the samples by conventional solid state method while Marrero-López synthesized the sample by freeze-dried precursor method and sintered it by conventional method. As shown in Fig. 6, curves present the similar thermal dependence trend. At low temperature (for the $LRS_{\|}$ sample, *T* below about 900 K, or $1000/T \geq 1.11$), the evolution appears to be linear, signature of a conventional Arrhenius-type behavior, whereas the high temperature evolution deviates from the Arrhenius behavior, which has been interpreted to be VTF-type [22]. But it should be noted that the conductivity has been significantly improved. The values are 2.2 × 10^{-3} S cm^{-1}, 0.017 S cm^{-1}, 0.058 S cm^{-1}, 0.09 S cm^{-1} at 500 °C, 600 °C, 700 °C and 800 °C, respectively, which are about three to five times as high as those obtained by Georges. The conductivity below 600 °C is also much higher than the results reported by Marrero-López.

The most probable reason for the increase of the electrical conductivity of the $LRS_{\|}$ is the negligible grain boundary effect in connection with its special microstructure. According to the brick layer model (Fig. 7(a)), grain boundaries in oxygen ion ceramic conductors increase the resistance due to grain boundary impurity phases and oxygen vacancies depletion in the space-charge layer

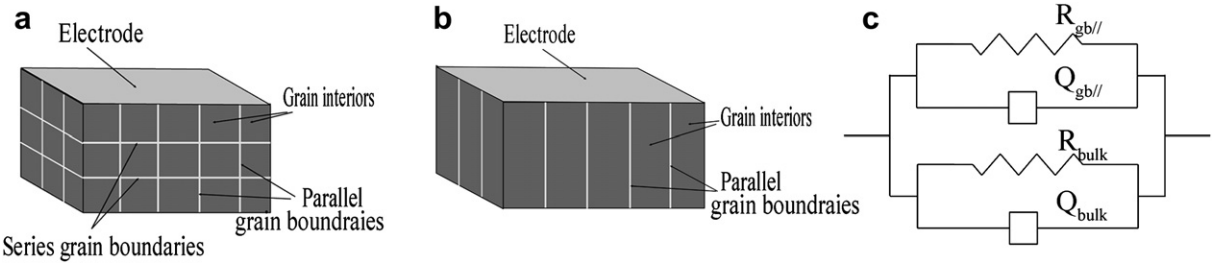

Fig. 7. Brick layer model for an electrolyte: conventionally sintered sample (a), $LRS_{\|}$ sample (b), equivalent circuit for $LRS_{\|}$ sample (c).

[13,27]. However, parallel grain boundaries and series grain boundaries play different roles in resistance. For $LRS_{\parallel}$ samples, the directions of grain boundaries are mainly from one electrode to another, as described above by SEM, which means most of them are parallel grain boundaries (Fig. 7(b)). Since oxygen ions transfer along the direction of parallel grain boundaries, the effect can be simplified to the equivalent circuit as Fig. 7(c). The approximate total resistance R can be got by the relation $1/R = 1/R_{gb\parallel} + 1/R_b$. Here R_b is the grain resistance, $R_{gb\parallel}$ denotes the parallel grain boundaries resistance. Suppose that the cross-sectional area of all parallel grain boundaries and all the grains are $A_{gb\parallel}$, A_b respectively, and that lengths of them are equal to be L, the equation can be written as $\sigma\cdot(A_b + A_{gb})/L = \sigma_b\cdot A_b/L + \sigma_{bg\parallel}\cdot A_{gb}/L$. For the $LRS_{\parallel}$ samples, the grains solidify to large blocks, and $A_{gb\parallel} << A_b$ is reasonable, so the resistance from parallel grain boundaries has little effect on the overall conductivity. That means the grain boundary blocking effect, whether it is from impurity phases or oxygen vacancies depletion or some others, is almost negligible for parallel grain boundaries, and hence $LRS_{\parallel}$ samples are of higher conductivity. In fact, as the solidification process is very complicated, some series grain boundaries exist inevitably, which reduce the electrical conductivity in some degree. Moreover, in most ionic conductor ceramics, the influence of grain boundary on the overall conductivity is little at high temperature but important at intermediate and low temperature [13]. From this point, why the conductivity of the $LRS_{\parallel}$ sample is much higher than that of samples synthesized by conventional sintering method, especially below 600 °C, can be understood.

For comparison, the conductivity in the direction perpendicular to the crystal solidification orientation of the laser sintered sample ($LRS_{\perp}$), as well as that of the SSR sample, was also studied in the same way as mentioned above. The impedance spectra of them at the same temperature are similar in shape, but different from that of the $LRS_{\parallel}$ sample. The main distinction is that all the spectra collected above 500 °C can be better fitted to $R(RQ)(RQ)$ than $R(RQ)$, and from the fitting results, values of the calculated capacitances are in the order of magnitude nF in accordance with mediate frequency (~KHz) and in the order of magnitude μF in accordance with low frequency (~Hz), indicating the grain boundary and the electrode response, respectively. Fig. 8 shows the measured and calculated spectra collected at 525 °C as examples, where two

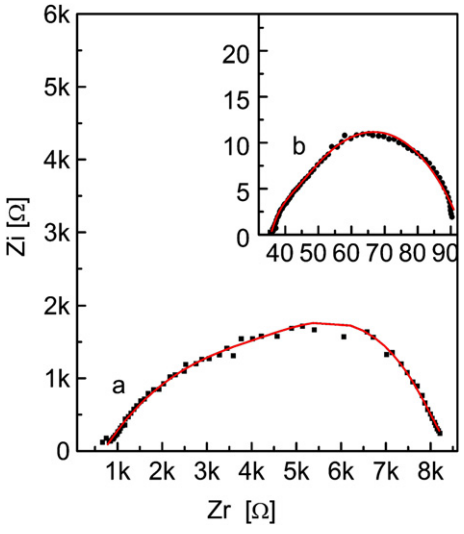

Fig. 8. Measured (scatter) and calculated (line) impedance spectra at 525 °C in dry air of $LRS_{\perp}$ LMW0.6 (a) and SSR LMW0.6 (b).

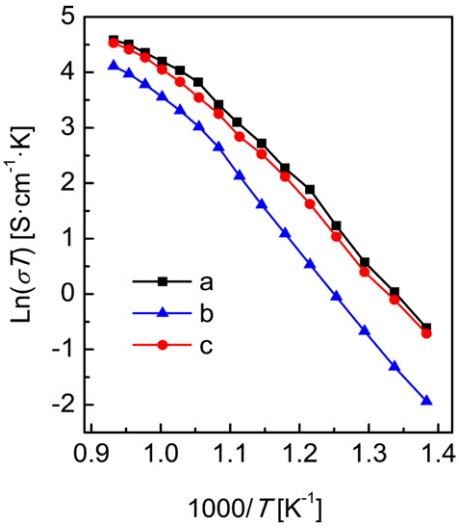

Fig. 9. Arrhenius plots in dry air of $LRS_{\parallel}$ LMW0.6 (a), $LRS_{\perp}$ LMW0.6 (b) and SSR LMW0.6 (c).

semi-circles are merged into a depressed arc in each spectrum. The conductivity values of the $LRS_{\perp}$ sample are calculated from its total resistance including grain and grain boundary effect, while those of the SSR sample are calculated only from the grain interior resistance. Arrhenius plots of the overall conductivity of $LRS_{\perp}$, $LRS_{\parallel}$ sample and the grain interior conductivity of the SSR sample are compared in Fig. 9. As shown in Fig. 9, the overall conductivity of LRS sample strongly depends on the measurement orientation and the conductivity values of the $LRS_{\parallel}$ sample are much higher than those in the perpendicular direction. Moreover, the overall conductivity values of the $LRS_{\parallel}$ sample are very close to the grain interior conductivity values of the SSR sample. These results further illuminate that the enhancement of electrical conductivity is due to reduced grain boundary resistances in the direction parallel to crystal solidification orientation.

4. Conclusions

$La_2Mo_{1.4}W_{0.6}O_9$ ceramic oxygen ion conductor has been successfully prepared by laser rapid solidification method with a CO_2 laser. The starting materials can melt fully, take reaction uniformly and solidify to ceramic with relatively density of 98.6% in a few minutes. The cubic β-$La_2Mo_2O_9$ structure is stabilized to room temperature and no phase transition is observed from room temperature to 800 °C. Due to the great temperature gradient in the rapid solidification process, the ceramic mainly solidifies against the direction of heat transfer to large blocks in the length of over 100 μm. When the two opposite surface sides perpendicular to the direction are connected to electrodes, the material exhibits high electrical conductivity in dry air, especially at the temperature below 600 °C. The conductivity values are 2.2×10^{-3} S cm^{-1}, 0.017 S cm^{-1}, 0.058 S cm^{-1}, 0.09 S cm^{-1} at 500 °C, 600 °C, 700 °C and 800 °C, respectively. The increase may be ascribed to the decrease of the grain boundary resistance, for most of them are parallel grain boundaries.

Acknowledgments

This work is financially supported by science & technology plan project of Henan province (12300410263) and science & technology research project of Zhengzhou city (112PPTGY219-9).

References

[1] A.J. Jacobson, Chem. Mater. 22 (2010) 660–674.
[2] J. Jacquens, D. Farrusseng, S. Georges, J.-P. Viricelle, C. Gaudillère, G. Corbel, P. Lacorre, Fuel Cells 10 (2010) 433–439.
[3] K. Huang, J. Wan, J.B. Goodenough, J. Mater. Sci. 36 (2001) 1093–1098.
[4] P. Pinet, J. Fouletier, S. Georges, Mater. Res. Bull. 42 (2007) 935–942.
[5] R. Polini, A. Falsetti, E. Traversa, O. Schäf, P. Knauth, J. Eur. Ceram. Soc. 27 (2007) 4291–4296.
[6] E. Courtin, P. Boy, T. Piquero, J. Vulliet, N. Poirot, C. Laberty-Robert, J. Power Sources 206 (2012) 77–83.
[7] J.X. Wang, Q. Wang, X.P. Wang, C. Li, Q.F. Fang, J. Mater. Sci. Technol. 24 (2008) 761–765.
[8] F. Deganello, G. Marcì, G. Deganello, J. Eur. Ceram. Soc. 29 (2009) 439–450.
[9] D. Marrero-López, J.C. Ruiz-Morales, P. Núñez, J.C.C. Abrantes, J.R. Frade, J. Solid State Chem. 177 (2004) 2378–2386.
[10] D. Marrero-López, J. Canales-Vazquez, J.C. Ruiz-Morales, A. Rodrigeez, J.T.S. Irivine, P. Núñez, Solid State Ionics 176 (2005) 1807–1816.
[11] D. Marrero-López, J. Peña-Martínez, D. Pérez-Coll, P. Núñez, J. Alloys Compd. 422 (2006) 249–257.
[12] J.G. Lee, S.H. Kim, H.H. Yoon, J. Nanosci. Nanotechnol. 12 (2012) 769–774.
[13] X. Guo, R. Waser, Prog. Mater. Sci. 51 (2006) 151–210.
[14] E.J. Liang, H.L. Huo, Z. Wang, M.J. Chao, J.P. Wang, Solid State Sci. 11 (2009) 139–143.
[15] J. Zhang, E.J. Liang, X.H. Zhang, J. Power Sources 195 (2010) 6758–6763.
[16] J.J. Zhang, J.M. Yu, M.J. Chao, E.J. Liang, M.Y. Li, D.C. Li, J. Mater. Sci. 47 (2011) 1554–1558.
[17] P. Lacorre, F. Goutenoire, O. Bohnke, R. Retoux, Y. Laligant, Nature 404 (2000) 856–858.
[18] F. Goutenoire, O. Isnard, E. Suard, O. Bohnke, Y. Laligant, R. Retoux, P. Lacorre, J. Mater. Chem. 11 (2001) 119–124.
[19] I.R. Evans, J.A.K. Howard, J.S.O. Evans, Chem. Mater. 17 (2005) 4074–4077.
[20] S. Georges, F. Goutenoire, O. Bohnke, M.C. Steilb, S.J. Skinnerc, H.-D. Wiemhöferd, P. Lacorre, J. New Mater. Electrochem. Syst. 7 (2004) 51–57.
[21] S. Georges, F. Goutenoire, Y. Laligant, P. Lacorre, J. Mater. Chem. 13 (2003) 2317–2321.
[22] S. Georges, O. Bohnke, F. Goutenoire, Y. Laligant, J. Fouletier, P. Lacorre, Solid State Ionics 177 (2006) 1715–1720.
[23] D. Marrero-López, J. Canales-Vázquez, W. Zhou, J.T.S. Irvine, P. Núñez, J. Solid State Chem. 179 (2006) 278–288.
[24] G. Corbel, Y. Laligant, F. Goutenoire, E. Suard, P. Lacorre, Chem. Mater. 17 (2005) 4678–4684.
[25] S. Georges, F. Goutenoire, P. Lacorre, M.C. Steil, J. Eur. Ceram. Soc. 25 (2005) 3619–3627.
[26] A. Selmi, G. Corbel, S. Kojikian, V. Voronkova, E. Kharitonova, P. Lacorre, Eur. J. Inorg. Chem. 11 (2008) 1813–1821.
[27] R. Meyer, X. Guo, R. Waser, Electrochem. Solid-State Lett. 8 (2005) E67–E69.